IEEE Access
Multidisciplinary ⋮ Rapid Review ⋮ Open Access Journal

Received June 13, 2020, accepted June 30, 2020, date of publication July 6, 2020, date of current version July 15, 2020.

Digital Object Identifier 10.1109/ACCESS.2020.3006929

Broadband Metamaterial Aperture Antenna for Coincidence Imaging in Terahertz Band

MENGRAN ZHAO, SHITAO ZHU, JUAN CHEN, (Member, IEEE), XIAOMING CHEN, (Senior Member, IEEE), AND ANXUE ZHANG

Key Laboratory of Multifunctional Materials and Structures, Ministry of Education, School of Information and Communication Engineering, Xi'an Jiaotong University, Xi'an 710049, China

Corresponding authors: Shitao Zhu (shitaozhu@xjtu.edu.cn) and Juan Chen (chen.juan.0201@xjtu.edu.cn)

This work was supported in part by the Shaanxi Provincial Natural Science Foundation under Grant 2017ZDXM-GY-009 and Grant 2020JM-078, in part by the China Postdoctoral Science Foundation under Grant 2017M613136, in part by the Natural Science Foundation of China under Grant 61501365, Grant 61801366, and Grant 61801368, and in part by the Fundamental Research Funds for the Central Universities under Grant xzy022019068.

ABSTRACT This paper proposes a broadband metamaterial aperture antenna (BMAA) with a large capacity, low correlation coefficients and high radiation efficiency for coincidence imaging in the terahertz band. The BMAA consists of a random modulated metamaterial aperture and a stripline structure as the feed system. Firstly, a metamaterial element complementary electric-inductor-capacitor (cELC) is designed and a metamaterial aperture is formed via randomly-distributed metamaterial elements with different resonant frequencies. By leveraging the amplitude and the phase modulation characteristics of the metamaterial elements, the BMAA can generate radiation patterns with low correlation coefficients in the range 240-340 GHz. In order to improve the feed efficiency, a stripline structural unit (SSU) is designed and analyzed using an even-odd mode analytical method, and a broadband feed system is designed by cascading SSUs. The performance of the BMAA, including the reflection coefficient, the radiation efficiency and the correlation coefficients of the radiation patterns at different frequencies are then evaluated. The BMAA can solve problems that exist for coincidence imaging, including a narrow working band, lack of measurement modes and low radiation efficiency and offers better results. Finally, a coincidence imaging experiment is implemented using the proposed BMAA and the original image is reconstructed successfully. All results are validated through simulations.

INDEX TERMS Metamaterial, port-diverse; frequency-diverse; coincidence imaging.

I. INTRODUCTION

With the rapid development of radio technology in recent years, bandwidth availability in the electronic-magnetic spectrum has become more and more scarce. Thus, terahertz frequencies have attracted much attention globally due to the advantages they offer, including a large capacity and the fact that electromagnetic waves in this band are harmless to the human body. Imaging and communication applications in the terahertz frequency range have become more prevalent, however, there are not many coincidence imaging applications in this range, due to a lack of devices and fabrication difficulties.

The requirements for a practical imaging system are that it is fast and accurate. The application of the metamaterials expands the potential of imaging systems by enabling design of a metaimager (i.e., a metamaterial-based microwave coincidence imaging system). A metaimager can be mainly divided into two types: cavity metaimagers and waveguide metaimagers. The most important part of a metaimager is the metamaterial aperture, which can couple energy from the feed system, modulate the phase or amplitude and generate radiation patterns with low correlation coefficients that can be used as measurement modes in coincidence imaging. There are two types of metamaterial apertures: frequency-diverse metamaterial apertures and polarization-sensitive metamaterial apertures. Frequency-diverse metamaterial apertures utilize differences in resonant frequencies of different metamaterial elements, resulting in different radiation patterns at different frequencies. Polarization-sensitive metamaterial apertures will generate different radiation patterns when stimulated by different polarization incident waves, based on each metamaterial element's sensitivity to polarization.

The associate editor coordinating the review of this manuscript and approving it for publication was Pu-Kun Liu.

The broadband metamaterial aperture antenna (BMAA) proposed in this paper is a type of frequency-diverse metamaterial aperture that can generate uncorrelated random beams at different frequencies.

In 2013, J. Hunt demonstrated that a low-profile aperture is capable of microwave computational imaging by leveraging metamaterials. This research firstly demonstrated the frequency-diverse characteristic of a metamaterial element complementary electric-inductor-capacitor (cELC). A metaimager was then presented, which was a single-pixel metamaterial implementation of holographic imaging at microwave frequencies [1]–[5]. This was the first realization of the waveguide metaimager type. In 2015, a mode-mixing cavity for computational imaging at microwave frequencies was proposed by T. Fromenteze, which was simple to fabricate, exhibited low losses, and was capable of generating several diverse measurement modes [6]–[8]. This was the first implementation of the cavity metaimager type. The core component of the cavity metaimager is an electrically-large rectangular cavity with one corner reshaped to catalyze mode mixing, which promises enough bandwidth to generate frequency-diverse radiation patterns. The characteristics of a traditional metamaterial are determined after processing, which limits their applications for some situations that require flexibility. However, the adoption of a tunable metamaterial accelerated the development of this type of metaimager [9]. In 2015, T. Sleasman proposed a metamaterial element containing two diodes connected to an external control circuit. In such a way that the resonance of the metamaterial element could be controlled by application of a bias voltage [10]. The diodes loaded on the tunable metamaterial can be regarded as a length-changeable structure that can control the resonant frequency, which offers the potential to design dynamic metamaterial apertures for microwave computational imaging.

In 2016, T. Sleasman used this tunable metamaterial to design a dynamically tunable impedance surface for a disordered cavity that can be used for microwave imaging [11]. The application of the tunable metamaterial has gradually become mainstream in metamaterial aperture design and many dynamic metaimagers for different imaging situations appeared during 2017 and 2018 [12]–[22]. In 2018, M. Zhao proposed a frequency-diverse transmission metamaterial aperture antenna for coincidence imaging, which is capable of generating a bunching random beam to improve the detection distance [23]. In 2019, a digitized metamaterial absorber-based compressive reflector antenna for high sensing capacity imaging was proposed by A. Molaei. The system is composed of a compressive reflector antenna with a surface that is specially tailored with digitized metamaterial absorbers [24].

However, all the research studies described above are based on utilizing the frequency characteristic of the metamaterial aperture. In order to generate additional measurement modes for imaging, many other methods have been proposed and the polarization dimension has also been concerned. In 2015, O. Yurduseven showed that increasing the number of receiving probe antennas could increase the effective aperture size, the number of measurement modes, and sampling of the scene [25]. In 2016, Z. Wu proposed a method to produce more effective radiation modes by rotating the metamaterial panel around the panel axis [26]. In 2017, T. Fromenteze proposed a polarimetric microwave imaging technique that exploits recent advances in computational imaging [27]. In 2018, O. Yurduseven proposed a dynamically reconfigurable metasurface aperture that can synthesize the required radiation pattern by converting the waveguide-mode to a free space radiation using a binary modulation scheme. Thus, microwave coincidence imaging can be applied at a single frequency [19]. In 2018, S. Zhu proposed a wideband frequency-polarization-diverse reflection metamaterial aperture in the Ka band, which can also be used to generate uncorrelated measurement modes from different polarization incident plane waves [28].

All these studies have contributed to a new design paradigm for designing the broadband metamaterial aperture antenna (BMAA) in coincidence imaging. Metamaterial-based coincidence imaging requires large numbers of uncorrelated measurement modes, which requires the metamaterial aperture antenna to have a wide bandwidth and low correlation coefficients between radiation patterns of different frequencies. In a previous study, a frequency-diverse metamaterial element complementary electric-inductor-capacitor (cELC) was designed [18]. In this paper, High-Frequency Structure Simulator (HFSS) software is used to design a metamaterial aperture by distributing the metamaterial elements randomly. Then, in order to obtain a good match across a wide bandwidth, a stripline structural unit (SSU) is designed and analyzed utilizing the even-odd mode analytical method. According to [29], the bandwidth of the stripline is theoretically wide. Therefore, the broadband feed system (i.e., the stripline structure with pontes) is designed by cascading SSUs and two feed ports of the feed system are designed in order to generate different radiation patterns at the same frequency. Finally, a BMAA with a large capacity, low correlation coefficients and high radiation efficiency is designed to generate random beams for coincidence imaging in the terahertz band. The radiation efficiency of the BMAA and the correlation coefficients of the radiation patterns at different frequencies of the proposed BMAA are also studied at the end of the paper. A coincidence imaging experiment using the proposed BMAA is also emulated and the results are provided. All results are validated through simulations.

II. DESIGN OF BMAA

The BMAA consists of a metamaterial aperture as the radiating module and a stripline structure as the broadband feeding system. A metallic sheet is also attached underneath the BMAA as a ground to ensure the efficiency. The overall schematic of the BMAA is shown in Fig. 1(c). The substrate is designed to be larger than the metamaterial aperture in order to eliminate diffraction interference.

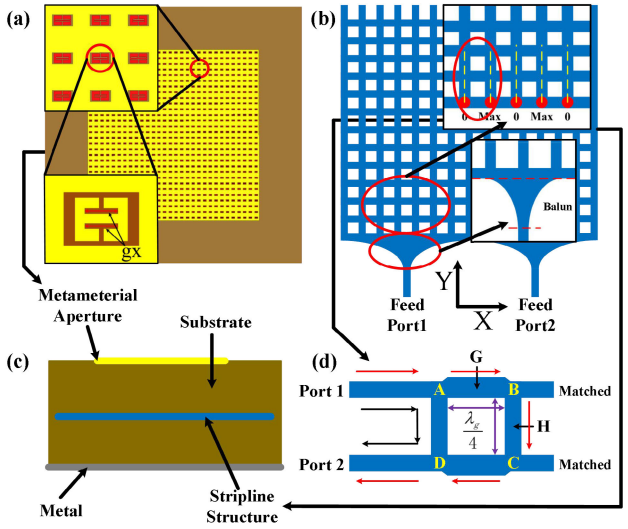

FIGURE 1. (a) Schematic of the metamaterial aperture; (b) Schematic of the stripline structure with two ports; (c) Schematic of the meta-material aperture antenna; (d) Equivalent model of the stripline structural unit (SSU).

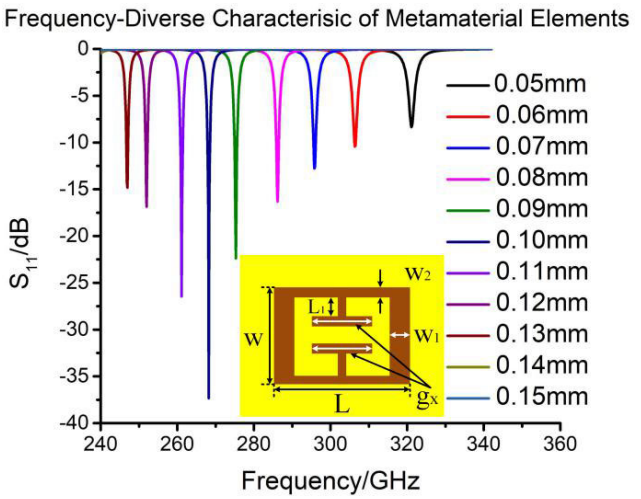

FIGURE 2. The structure and frequency-diverse characteristic of cELC.

The size of the substrate is 18 mm × 18 mm and the size of the metamaterial aperture is 15 mm × 15 mm. The length of the stripline structure is chosen as 15 mm, based on the size of the metamaterial aperture. The stripline structure is inserted in the substrate and the distance between the stripline structure and the metallic sheet is 0.1 mm (i.e., the stripline structure is approximately in the middle of the substrate). The permittivity of the substrate is 2.2, the loss tangent (tanδ) is 0.001 and the thickness of the substrate is 0.21 mm.

A. DESIGN OF METAMATERIAL ELEMENT AND APERTURE

In a metamaterial aperture, a broadband guided electromagnetic wave transmitted by the stripline structure will be coupled by cELCs resonating at different frequencies [30]–[33], where each cELC can be regarded as an element of the antenna array with a specific amplitude and phase modulation characteristic. Different radiation patterns will be generated at different frequencies due to the random distribution of different metamaterial elements.

The key principle of a metamaterial aperture is the design of metamaterial elements with a range of different resonance frequencies. Fig. 2 shows the designed metamaterial element cELC working in the terahertz band. The parameters of the cELC are as follows. L = 0.22 mm, W = 0.12 mm, W_1 = 0.02 mm, W_2 = 0.01mm, L_1 = 0.035 mm. The slots of the cELC can be regarded as magnetic dipoles or electric dipoles, and thus the length and the width of the slot will influence the resonant frequency of the whole structure. By using a Floquet port to simulate periodical patterns, the metamaterial element model can be built in the HFSS. The simulation results show that by altering parameter g_x the resonant frequency can be changed when the metamaterial element is working in the terahertz band. For example, when g_x is changed from 0.05 mm to 0.15 mm, the resonant frequency of the metamaterial element is shown to decrease from 340 GHz to 240 GHz.

The BMAA is actually a microstrip antenna, so 30 different metamaterial elements with g_x values from 0.05 mm to 0.15 mm (900 in total) are selected and etched on the standard microstrip randomly to form the metamaterial aperture, as shown in Fig. 1(a). As shown in Fig. 2, Each g_x value corresponds to a resonant frequency, meaning that metamaterial elements with different values of g_x will couple energy from the feed system at different frequencies. Due to the randomness of different metamaterial elements, different radiation patterns will be generated at different frequencies. Thus, the wide bandwidth of the BMAA offers abundant frequency-diverse radiation patterns which will act as necessary measurement modes for coincidence imaging.

B. DESIGN OF THE STRIPLINE STRUCTURE

In order the achieve broadband impedance matching, an SSU is designed as shown in Fig. 1(d) and analyzed by utilizing the even-odd mode analytical method. The stripline structure is then designed by cascading SSUs and the energy will be coupled from the stripline structure to the resonant metamaterial elements.

The pontes connecting the feed port and the stripline structure shown in Fig. 1(b) can be regarded to be acting as a balun. The curve of the pontes is optimized using the HFSS in order to guarantee that the width of the stripline will change gradually. The objective of the optimization is to reduce the reflection coefficient to zero, which is reflected in HFSS by a value of S_{11} that is lower than −10dB. The impedance of the stripline corresponds to the width of the stripline. As can be seen in equation (1), when the impedance of the stripline changes gradually, the reflecting coefficient Γ can be controlled to be approximately zero.

$$\Gamma = \frac{Z_L - Z_C}{Z_L + Z_C} \tag{1}$$

The electric field distribution of the stripline structure is shown in the magnified portion of the Fig. 1(b), which is acquired through the HFSS. Using this electric field distribution, the stripline structure can be split in the middle of the stripline along the Y axis into the stripline structural unit (SSU), as shown in Fig. 1(d). It can be seen from this figure that the SSU has two ports on the left side and matched loads on the right side. The lengths of paths AB, BC, CD and AD are all $\lambda_g/4$, where λ_g represents the wavelength of the central frequency. The parameters G and H represent the admittance of the corresponding stripline. The equivalent model of the SSU can be regarded as a coupler, as the purpose of the unit is to transmit the power from the port (i.e., port1 or port2) without echoes.

The even-odd mode analytical method is utilized to analyze the SSU. When a unit is simulated by even-mode excitation as shown in Fig. 3(a), a magnetic wall should be added and the equivalent circuit is as shown in Fig. 3(c). Similarly, an electric wall should be added when simulated by odd-mode excitation as shown in Fig. 3(b), and its equivalent circuit is as shown in Fig. 3(d).

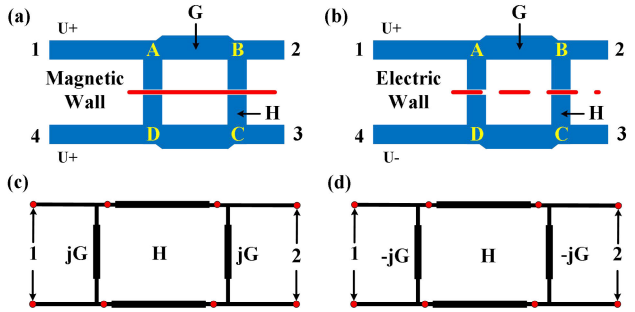

FIGURE 3. (a) Simulated by even-mode excitation; (b) Simulated by odd-mode excitation; (c) Equivalent circuit of the SSU under even-mode excitation; (d) The equivalent circuit of the SSU under odd-mode excitation.

Using the S matrixes of both modes, the voltage at ports 1 and 4 can be expressed by equations (2) and (3) for the even-mode and odd-mode, respectively:

$$U_{1even} = U_{4even} = U_0 \left[1 + \frac{j\left(\frac{G^2}{H} + \frac{1}{H} - H\right)}{-\frac{2G}{H} + j\left(H + \frac{1}{H} - \frac{G^2}{H}\right)} \right] \quad (2)$$

$$U_{1odd} = -U_{4odd} = U_0 \left[1 + \frac{j\left(\frac{G^2}{H} + \frac{1}{H} - H\right)}{\frac{2G}{H} + j\left(H + \frac{1}{H} - \frac{G^2}{H}\right)} \right] \quad (3)$$

The conditions $U_1 = 2U_0$ and $U_4 = 0$ should be followed if it is expected that there will be no echoes into ports 1 and 4. Thus, the relationship between G and H can be obtained as shown in equation (4).

$$G^2 + 1 = H^2 \quad (4)$$

Through the analysis above and the optimization of HFSS, the width of the stripline structure along the X axis is found to be 0.2 mm and the width of the stripline structure along the Y axis is found to be 0.24 mm as shown in Fig. 1(b). Due to the existence of the pontes and the tolerance of the balun to the frequency offset, the proposed stripline structure can be considered as a broadband feed system.

Two feed ports are designed for the stripline structure to validate the port-diverse characteristic, as shown in Fig. 1(b). Different ports will generate different radiation patterns at the same frequency, which can offer an increased number of measurement modes for coincidence imaging. The independence between multiple ports is also verified through the two feed ports.

C. COINCIDENCE IMAGING USING THE BMAA

Random reference radiation modes (complex radiation patterns of the BMAA at different center frequencies) are required in the coincidence imaging process, which should ideally be independent to each other. These random reference radiation modes are used for the measurements to ensure that the measurements are uncorrelated. The following measurement equation matrix will be formed using all of the collected measurement data:

$$\begin{bmatrix} S_t(t_1) \\ S_t(t_2) \\ \vdots \\ S_t(t_M) \end{bmatrix} = \begin{bmatrix} S_R(I_1, t_1) & \cdots & S_R(I_Q, t_1) \\ S_R(I_1, t_2) & \cdots & S_R(I_Q, t_2) \\ \vdots & \vdots & \vdots \\ S_R(I_1, t_M) & \cdots & S_R(I_Q, t_M) \end{bmatrix} \begin{bmatrix} \sigma(I_1) \\ \sigma(I_2) \\ \vdots \\ \sigma(I_Q) \end{bmatrix} + \begin{bmatrix} n(t_1) \\ n(t_2) \\ \vdots \\ n(t_M) \end{bmatrix} \quad (5)$$

where $S_t(T_m)$ is the measurement data, $S_R(I_q, t_m)$ is the distribution of the measurement mode (generated by the BMAA) in the imaging plane, I_q represents the discrete imaging point, $\sigma(I_q)$ is the scatting coefficient at the I_qth imaging point, t_m represents the test index and $n(t_m)$ is the measurement noise.

Equation (5) can be solved using the fast iterative shrinkage threshold algorithm (FISTA) method [34] or the conjugate gradient least squares algorithm (CGLS) [35] with high efficiency. Hence, a high-quality image can be reconstructed by using all the measurement data together.

III. SIMULATIONS AND IMAGING EXPERIMENT

A. THE BMAA

The HFSS software is utilized to validate the proposed BMAA. As shown in Fig. 4(a), the reflection coefficients S_{11} and S_{22} have an amplitude of -10 dB or lower between 240-320 GHz, which validates the broadband characteristic of the stripline structure (i.e., the feed system). The mutual coupling S_{21} shown in Fig. 4(a) is -15 dB or lower within the working band, which confirms that there is good isolation between the two feed ports. From the results above, it can be seen that the BMAA is successfully fed by the stripline structure in the terahertz band.

The BMAA is simulated at several frequencies in the HFSS and the radiation efficiency (i.e., the ratio of the radiated

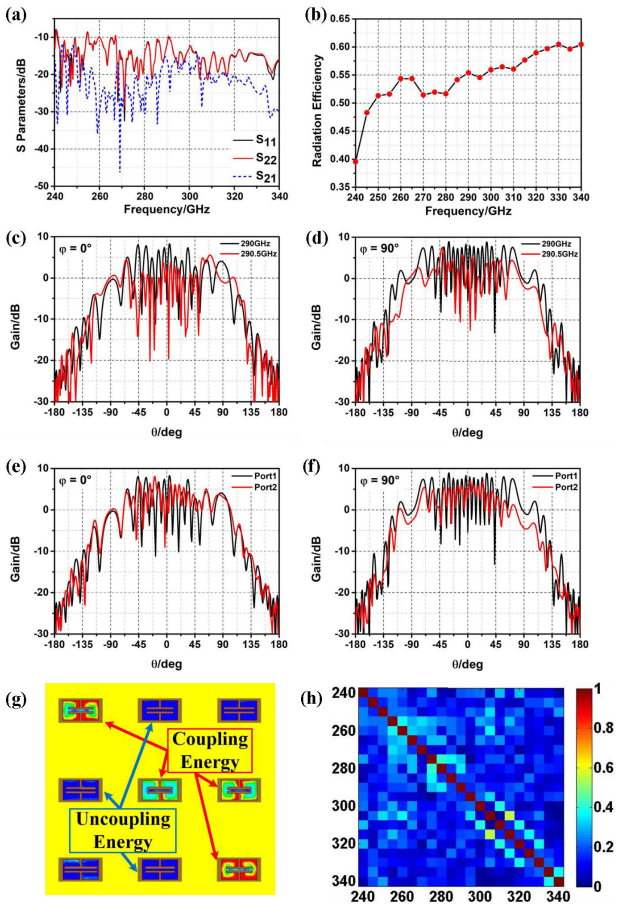

FIGURE 4. (a) Reflection coefficients (S_{11} and S_{22}) and mutual coupling (S_{21}) of the BMAA; (b) Radiation efficiency of the BMAA at several frequencies; Radiation patterns of different frequencies (c) ($\varphi = 0°$); (d) ($\varphi = 90°$); Radiation patterns of 290 GHz when different ports are simulated (e) ($\varphi = 0°$); (f) ($\varphi = 90°$). (g) Electric field distribution of the metamaterial elements when simulated at 290 GHz; (h) Correlation coefficients of radiation patterns at different frequencies.

power to the input power) of the BMAA calculated by the HFSS is shown in Fig. 4(b). The radiation efficiency of the metamaterial aperture between 240-340 GHz is in the range 0.4-0.6, which is quite high. As shown in Fig. 4(c) and Fig. 4(d), the radiation patterns of two different frequencies (290 GHz and 290.5 GHz) are both different, which illustrates the frequency-diverse characteristic of the BMAA. The port-diverse characteristic of the BMAA is also studied. Fig. 4(e) and Fig. 4(f) show that the radiation patterns of two different feed ports (feed port1 and feed port2) at the same frequency (290 GHz) are different, which proves the feasibility of a multiport stripline structure design.

When the BMAA is simulated at the feed ports, energy is transmitted by the pontes and the stripline structure to the metamaterial aperture. The metamaterial elements will couple energy from the stripline structure at each element's specific resonant frequency. As shown in Fig. 4(g), when the BMAA is simulated at 290 GHz, any metamaterial element with S_{11} under -10 dB will couple energy from the stripline structure. The lower the value of S_{11}, the more energy that will be coupled. In contrast, metamaterial elements which are not resonant at 290 GHz will not couple energy. These analyses are illustrated by the metamaterial elements shown in Fig. 4(g). As shown in Fig. 4(h), the correlation coefficients of the radiation patterns at different frequencies are studied. The correlation coefficients show the incoherence of different frequencies' radiation patterns. From Fig. 4(h), the correlation coefficients will be mostly under 0.3 when the frequency interval is set at 5 GHz (1.7% relative bandwidth), which promises good results in the coincidence imaging implementation [36]. Additionally, the correlation coefficients of radiation patterns of different ports is 0.271, which offers significant improvement of the measurement modes at the same working frequency.

B. IMAGING EXPERIMENT

A typical scene of coincidence imaging experiment is shown in Fig. 5. The BMAA was used as the transmitting antenna and the horn antenna was used as the receiving antenna. The The target was in the 3dB beam-width of the coherent transmitting aperture and contained several discrete points. The size of the BMAA was 15mm×15mm. The imaging distance was approximately 150mm. The imaging plane was in the pitch-azimuth plane. The imaging plane contained $K_1 \times K_2$ imaging cells and was equally discretized, where $K_1 = 5$ was in the azimuth direction and $K_2 = 5$ was in the pitch direction. The side length of the imaging targets was 2 mm (approximately 1/5 of the 3dB beam-width of the coherent transmitting aperture with the same size as the BMAA) in both directions.

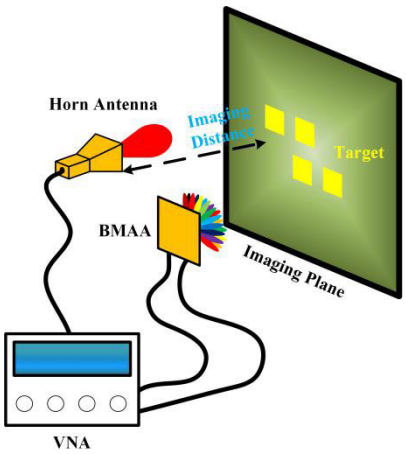

FIGURE 5. Typical scene of coincidence imaging experiment.

For the imaging experiment using the BMAA, the complex radiation patterns of the BMAA at different center frequencies were obtained in advance by simulations. The image data was obtained according to the schematic shown in Fig. 6(a), which is processed in MATLAB.

The distance resolution of the BMAA was $\delta_d = C/2B$, where C is the light velocity and B is the bandwidth of the detection signal. However, the phase differential should be revised to reduce the diversity of the BMAA [36], since the

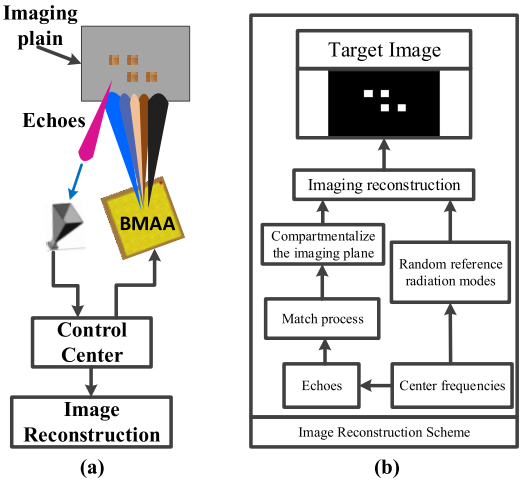

FIGURE 6. (a) Architecture of the imaging experiment, (b) Flow chart of the coincidence imaging with the BMAA.

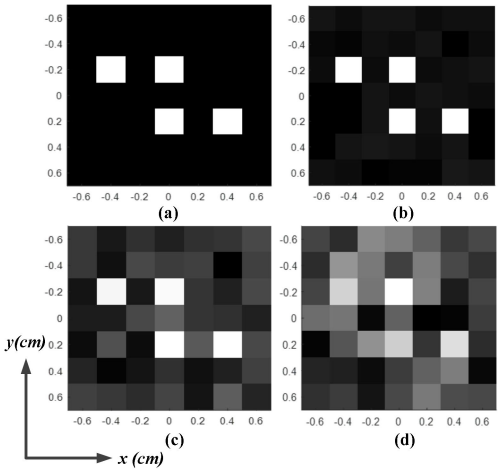

FIGURE 7. Comparisons of the imaging results; (a) Original image. (b) Reconstructed image with an SNR of 20 dB. (c) Reconstructed image with an SNR of 12 dB. (d) Reconstructed image with an SNR of 6 dB.

phase is randomly modulated by the aperture. The azimuth resolution depends on the signal-to-noise ratio (SNR) of the measurement data and the size of the aperture. The 3dB beamwidth is the basics azimuth resolution, which can be improved when the SNR increases.

A flow chart of the coincidence imaging with the BMAA is shown in Fig. 6(b). The match process step includes target distance estimation and requires a match between the echoes and the random reference radiation modes. As shown in Fig. 7, a high-quality image can be reconstructed when the SNR of the test data is larger than 20dB. The quality of the reconstructed image declines as the SNR of the test data reduces, and the reconstructed image is completely blurred when the SNR is lower than 6dB.

A comparison between the proposed BMAA and previous works has been given as shown in Table 1. The number of measurement modes (m) is related to the working bandwidth (w) and the minimum low-correlated frequency gap (g). The measurement modes number shown in Table 1 is calculated according to $m = w/g$. As shown in Table 1, compared

TABLE 1. Comparison of proposed and previous metamaterial antenna.

Work	Working Band	Aperture Size	Measurement Modes
Ref. [1]	18.5-25 GHz	40cm*2cm	217
Ref. [6]	18-26.5 GHz	20cm*20cm	804
Ref. [7]	17.5-26.5 GHz	20cm*20cm	199
Ref. [12]	17.5-26.5 GHz	14cm*14cm	625
Ref. [37]	75-110 GHz	4cm*4cm	200
Proposed BMAA	240-340 GHz	1.8cm*1.8cm	1350

with previous works, the proposed BMAA has the most measurement modes and the widest working bandwidth while containing the smallest aperture size, which promises good performance in the implementation of the coincidence imaging.

IV. CONCLUSION

In this paper, a broadband metamaterial aperture antenna (BMAA) design was proposed which has a large capacity, low correlation coefficients and high radiation efficiency for coincidence imaging in the terahertz band. The metamaterial aperture consisted of 30 types of cELCs (900 in total) with different resonant frequencies which generate different radiation patterns at different frequencies in order to provide the required frequency-diverse characteristic. A multiport stripline structure was also designed to feed the metamaterial aperture which could generate different radiation patterns when stimulated at different ports, which provided the required port-diverse characteristic. The stripline structural unit (SSU) was analyzed utilizing the even-odd mode analytical method and a broadband feed system was designed by cascading SSUs. Simulation results showed that the BMAA is well-fed between 240 GHz-340 GHz. The radiation efficiency of the BMAA was between 0.4 and 0.6 within the working bandwidth calculated using the HFSS, which can be considered to be quite high for metamaterial aperture antennas. The correlation coefficients of the radiation patterns at different frequencies were below 0.3 in most cases, which proved that there are low correlation coefficients between different radiation patterns. Various radiation patterns can be used for the different measurement modes, thus ensuring the feasibility of coincidence imaging [28]. A coincidence imaging experiment using this BMAA was also emulated. The experiment showed that the image could be reconstructed with high quality when the SNR of the test data was above 20 dB. All results were validated through simulations.

ACKNOWLEDGMENT

The authors acknowledge Sen Yan, Qinlong Li, Qian Yang, Ming Zhang, Hongyu Shi and Xiaobo Liu from Xi'an Jiaotong University for theoretical assistance. The authors also acknowledge Luyi Wang, Gantao Peng for technical support.

REFERENCES

[1] J. Hunt, T. Driscoll, A. Mrozack, G. Lipworth, M. Reynolds, D. Brady, and D. R. Smith, "Metamaterial apertures for computational imaging," *Science*, vol. 339, no. 6117, pp. 310–313, Jan. 2013.

[2] G. Lipworth, A. Mrozack, J. Hunt, D. L. Marks, T. Driscoll, D. Brady, and D. R. Smith, "Metamaterial apertures for coherent computational imaging on the physical layer," *J. Opt. Soc. Amer. A, Opt. Image Sci.*, vol. 30, no. 8, pp. 1603–1612, 2013.

[3] G. Lipworth, J. Hunt, A. Mrozack, D. Brady, and D. R. Smith, "Simulations of 2D metamaterial apertures for coherent computational imaging," in *Proc. COMCAS*, Tel Aviv, Israel, Oct. 2013, pp. 1–4.

[4] J. Hunt, J. Gollub, T. Driscoll, G. Lipworth, A. Mrozack, M. S. Reynolds, D. J. Brady, and D. R. Smith, "Metamaterial microwave holographic imaging system," *J. Opt. Soc. Amer. A, Opt. Image Sci.*, vol. 31, no. 10, pp. 2109–2119, Oct. 2014.

[5] G. Lipworth, A. Rose, O. Yurduseven, V. R. Gowda, M. F. Imani, H. Odabasi, P. Trofatter, J. Gollub, and D. R. Smith, "Comprehensive simulation platform for a metamaterial imaging system," *Appl. Opt.*, vol. 54, no. 31, pp. 9343–9353, 2015.

[6] O. Yurduseven, V. R. Gowda, J. N. Gollub, and D. R. Smith, "Printed aperiodic cavity for computational and microwave imaging," *IEEE Microw. Wireless Compon. Lett.*, vol. 26, no. 5, pp. 367–369, May 2016.

[7] T. Fromenteze, O. Yurduseven, M. F. Imani, J. Gollub, C. Decroze, D. Carsenat, and D. R. Smith, "Computational imaging using a mode-mixing cavity at microwave frequencies," *Appl. Phys. Lett.*, vol. 106, no. 19, May 2015, Art. no. 194104.

[8] M. F. Imani, T. Sleasman, J. N. Gollub, and D. R. Smith, "Analytical modeling of printed metasurface cavities for computational imaging," *J. Appl. Phys.*, vol. 120, no. 14, Oct. 2016, Art. no. 144903.

[9] I. B. Vendik, O. G. Vendik, M. A. Odit, D. V. Kholodnyak, S. P. Zubko, M. F. Sitnikova, P. A. Turalchuk, K. N. Zemlyakov, I. V. Munina, D. S. Kozlov, V. M. Turgaliev, A. B. Ustinov, Y. Park, J. Kihm, and C.-W. Lee, "Tunable metamaterials for controlling THz radiation," *IEEE Trans. THz Sci. Technol.*, vol. 2, no. 5, pp. 538–549, Sep. 2012.

[10] T. Sleasman, M. F. Imani, J. N. Gollub, and D. R. Smith, "Dynamic metamaterial aperture for microwave imaging," *Appl. Phys. Lett.*, vol. 107, no. 20, Nov. 2015, Art. no. 204104.

[11] T. Sleasman, M. F. Imani, J. N. Gollub, and D. R. Smith, "Microwave imaging using a disordered cavity with a dynamically tunable impedance surface," *Phys. Rev. A, Gen. Phys.*, vol. 6, no. 5, Nov. 2016, Art. no. 054019.

[12] D. L. Marks, O. Yurduseven, and D. R. Smith, "Cavity-backed metasurface antennas and their application to frequency diversity imaging," *J. Opt. Soc. Amer. A, Opt. Image Sci.*, vol. 34, no. 4, pp. 472–480, 2017.

[13] O. Yurduseven, P. Flowers, S. Ye, D. L. Marks, J. N. Gollub, T. Fromenteze, B. J. Wiley, and D. R. Smith, "Computational microwave imaging using 3D printed conductive polymer frequency-diverse metasurface antennas," *IET Microw., Antennas Propag.*, vol. 11, no. 14, pp. 1962–1969, Nov. 2017.

[14] T. Zvolensky, J. N. Gollub, D. L. Marks, and D. R. Smith, "Design and analysis of a W-Band metasurface-based computational imaging system," *IEEE Access*, vol. 5, pp. 9911–9918, 2017.

[15] A. Pedross-Engel, C. M. Watts, D. R. Smith, and M. S. Reynolds, "Enhanced resolution stripmap mode using dynamic metasurface antennas," *IEEE Trans. Geosci. Remote Sens.*, vol. 55, no. 7, pp. 3764–3772, Jul. 2017.

[16] T. Sleasman, M. Boyarsky, L. Pulido-Mancera, T. Fromenteze, M. F. Imani, M. S. Reynolds, and D. R. Smith, "Experimental synthetic aperture radar with dynamic metasurfaces," *IEEE Trans. Antennas Propag.*, vol. 65, no. 12, pp. 6864–6877, Dec. 2017.

[17] X. Q. Chen, X. Wan, and T. J. Cui, "A novel leaky-wave antenna based on 1-bit coding metamaterial," in *Proc. 6th Asia–Pacific Conf. Antennas Propag. (APCAP)*, Xi'an, China, Oct. 2017, pp. 1–3.

[18] M. Zhao, S. Zhu, B. Wu, and A. Zhang, "Simulations and measurement of 2D metamaterial aperture antenna," in *Proc. 6th Asia–Pacific Conf. Antennas Propag. (APCAP)*, Xi'an, China, Oct. 2017, pp. 1–3.

[19] O. Yurduseven, D. L. Marks, T. Fromenteze, and D. R. Smith, "Dynamically reconfigurable holographic metasurface aperture for a mills-cross monochromatic microwave camera," *Opt. Express*, vol. 26, no. 5, pp. 5281–5291, 2018.

[20] A. V. Diebold, M. F. Imani, T. Sleasman, and D. R. Smith, "Phaseless computational ghost imaging at microwave frequencies using a dynamic metasurface aperture," *Appl. Opt.*, vol. 57, no. 9, pp. 2142–2149, 2018.

[21] B. Michael, T. Sleasman, L. Pulido-Mancera, A. V. Diebold, M. F. Imani, and D. R. Smith, "Single-frequency 3D synthetic aperture imaging with dynamic metasurface antennas," *Appl. Opt.*, vol. 57, no. 15, pp. 4123–4734, 2018.

[22] M. F. Imani, T. Sleasman, and D. R. Smith, "Two-dimensional dynamic metasurface apertures for computational microwave imaging," *IEEE Antennas Wireless Propag. Lett.*, vol. 17, no. 12, pp. 2299–2303, Dec. 2018.

[23] M. Zhao, S. Zhu, X. Chen, J. Li, D. Hu, L. Wang, and A. Zhang, "Frequency-diverse transmission metamaterial aperture with a bunching random beam," *IEEE Antennas Wireless Propag. Lett.*, vol. 17, no. 6, pp. 1029–1033, Jun. 2018.

[24] A. Molaei, J. Heredia-Juesas, G. Ghazi, J. Vlahakis, and J. A. Martinez-Lorenzo, "Digitized metamaterial absorber-based compressive reflector antenna for high sensing capacity imaging," *IEEE Access*, vol. 7, pp. 1160–1173, 2019.

[25] O. Yurduseven, J. Gollub, H. Odabasi, M. F. Imani, G. Lipworth, A. Rose, P. Trofetter, and D. R. Smith, "Probe configuration study for the metamaterial aperture imager," in *Proc. Eur. Conf. Antennas Propag. (EuCAP)*, Aug. 2015, pp. 1–4.

[26] Z. Wu, L. Zhang, H. Liu, and N. Kou, "Enhancing microwave metamaterial aperture radar imaging performance with rotation synthesis," *IEEE Sensors J.*, vol. 16, no. 22, pp. 8035–8043, Nov. 2016.

[27] T. Fromenteze, O. Yurduseven, M. Boyarsky, J. Gollub, D. L. Marks, and D. R. Smith, "Computational polarimetric microwave imaging," *Opt. Express*, vol. 25, no. 22, pp. 27488–27505, 2017.

[28] S. Zhu, X. Dong, Y. He, M. Zhao, G. Dong, X. Chen, and A. Zhang, "Frequency-polarization-diverse aperture for coincidence imaging," *IEEE Microw. Wireless Compon. Lett.*, vol. 28, no. 1, pp. 82–84, Jan. 2018.

[29] G. Arun Kumar and D. R. Poddar, "Broadband rectangular waveguide to suspended stripline transition using dendritic structure," *IEEE Microw. Wireless Compon. Lett.*, vol. 26, no. 11, pp. 900–902, Nov. 2016.

[30] F. Falcone, T. Lopetegi, M. A. G. Laso, J. D. Baena, J. Bonache, M. Beruete, R. Marqués, F. Martín, and M. Sorolla, "Babinet principle applied to the design of metasurfaces and metamaterials," *Phys. Rev. Lett.*, vol. 93, no. 19, Nov. 2004, Art. no. 197401.

[31] T. H. Hand, J. Gollub, S. Sajuyigbe, D. R. Smith, and S. A. Cummer, "Characterization of complementary electric field coupled resonant surfaces," *Appl. Phys. Lett.*, vol. 93, no. 21, p. 4184, Nov. 2008.

[32] C. Rockstuhl, C. Menzel, S. Mühlig, J. Petschulat, C. Helgert, C. Etrich, A. Chipouline, T. Pertsch, and F. Lederer, "Scattering properties of meta-atoms," *Phys. Rev. B, Condens. Matter*, vol. 83, no. 24, Jun. 2011, Art. no. 245119.

[33] X. Liu, J. Zhang, W. Li, R. Lu, S. Zhu, Z. Xu, and A. Zhang, "An analytical design of cross polarization converter based on the gangbuster metasurface," *IEEE Antennas Wireless Propag. Lett.*, vol. 16, pp. 1028–1031, 2017.

[34] M. Zulfiquar Ali Bhotto, M. O. Ahmad, and M. N. S. Swamy, "An improved fast iterative shrinkage thresholding algorithm for image deblurring," *SIAM J. Imag. Sci.*, vol. 8, no. 3, pp. 1640–1657, Jan. 2015.

[35] R. He, A. F. Molisch, F. Tufvesson, Z. Zhong, B. Ai, and T. Zhang, "Vehicle-to-vehicle propagation models with large vehicle obstructions," *IEEE Trans. Intell. Transp. Syst.*, vol. 15, no. 5, pp. 2237–2248, Oct. 2014.

[36] S. Zhu, M. Zhao, X. Dong, H. Shi, R. Lu, X. Chen, and A. Zhang, "Differential coincidence imaging with frequency diverse aperture," *IEEE Antennas Wireless Propag. Lett.*, vol. 17, no. 6, pp. 964–968, Jun. 2018.

[37] T. Zvolensky, V. R. Gowda, J. Gollub, D. L. Marks, and D. R. Smith, "W-band sparse imaging system using frequency diverse cavity-fed metasurface antennas," *IEEE Access*, vol. 6, pp. 73659–73668, 2018.

MENGRAN ZHAO was born in Shijiazhuang, Hebei, China, in 1993. He received the B.S. degree in information engineering from Xi'an Jiaotong University, Xi'an, China, in 2016, where he is currently pursuing the Ph.D. degree in electronic science and technology. His research interests mainly include metasurface antenna with bunching random beams for coincidence imaging, mm-wave antenna design, and polarization-sensitive metamaterial theory.

SHITAO ZHU received the B.S. degree in electronic information science and technology from Lanzhou University, Lanzhou, China, in 2005, and the M.S. degree in information and communication engineering and the Ph.D. degree in electronic science and technology from Xi'an Jiaotong University, in 2008 and 2016, respectively. From 2008 to 2012, he was a System Engineer with ZTE Corporation, Xi'an. He is currently an Associate Research Fellow with the School of Information and Communication Engineering, Xi'an Jiaotong University. His research interests include the metamaterial antenna, radar signal processing, and microwave coincidence imaging.

JUAN CHEN (Member, IEEE) received the Ph.D. degree in electro-magnetic and microwave engineering from Xi'an Jiaotong University, Xi'an, China, in 2008. From 2016 to 2017, she was a Visiting Researcher with the Department of Electrical and Computer Engineering, Duke University, Durham, NC, USA, under the financial support from the China Scholarship Council. She is currently a Professor with the Shenzhen Research School, Xi'an Jiaotong University, where she is also with the School of Electronic and Information Engineering. Her current research interests include numerical electro-magnetic methods, advanced antenna design, and grapheme theory and applications.

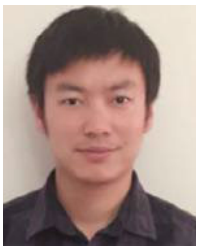

XIAOMING CHEN (Senior Member, IEEE) received the B.S. degree in electrical engineering from Northwestern Polytechnical University, Xi'an, China, in 2006, and the M.S. and Ph.D. degrees in electrical engineering from the Chalmers University of Technology, Gothenburg, Sweden, in 2007 and 2012, respectively. From 2013 to 2014, he was a Postdoctoral Researcher with the Chalmers University of Technology. From 2014 to 2017, he was with Qam-com Research and Technology AB, Gothenburg. Since 2017, he has been a Professor with Xi'an Jiaotong University, Xi'an. His research interests include MIMO antennas, over-the-air testing, reverberation chambers, and hardware impairments and mitigation.

ANXUE ZHANG received the B.S. degree in electrical engineering from Henan Normal University, in 1996, and the M.S. and Ph.D. degrees in electromagnetic and microwave engineering from Xi'an Jiaotong University, in 1999 and 2003, respectively. He is currently a Professor with Xi'an Jiaotong University. His main research fields include metamaterials, RF and microwave circuit design, antenna, and electromagnetic wave propagation.